A Multidimensional Scaling Optimization and Fusion Approach For the Unsupervised Change Detection Problem in Remote Sensing Images

Redha Touati[1], Max Mignotte[1]
[1] Département d'Informatique et de Recherche Opérationnelle (DIRO), Université de Montréal
e-mail: touatire@iro.umontreal.ca

***Abstract*— It is generally well known that the overall performance of the most widely used types of unsupervised change detection methods, based on the luminance pixel-wise difference, is mainly relied on the quality of the so-called difference image and the accuracy of the classification method. In order to address these two issues, this work proposes to first estimate, a new and robust similarity feature map, playing the same role as the difference image, by specifying a set of constraints expressed for each pair of pixels existing in the multitemporal images. As a consequence, the proposed change detection method does not require any preprocessing step of the multitemporal images such as radiometric correction/normalization. In addition, input data can be acquired from different sensors. The quadratic complexity in the number of pixels of this new similarity feature map, between the multitemporal images, is reduced to a linear complexity procedure thanks to the FastMap-based optimization algorithm. Second, in order to achieve more robustness, changes are then identified, from this similarity feature map, by combining (fusing) the results of different automatic thresholding algorithms. Experimental results confirm the robustness of the proposed approach.**

***Keywords*— Change detection, Data fusion, Multidimensional scaling, Multitemporal multimodal images, Thresholding algorithms.**

I. Introduction

Image change detection, in remote sensing, is a process whose purpose is to analyze two or several images (possibly generated by different sensors and/or from different spectral bands) of the same geographical area, at different times, in order to identify any changes that may have occurred between them.

In the lase decades, it has attracted widespread interest as it is particularly useful for a wide range of applications in remote sensing including, deforestation, land cover changes, impact of natural disasters like tsunamis, earthquakes, natural resource management, military purposes, vegetation or urban development analysis or agricultural monitoring, to name a few. Let us also mention that change detection techniques can also be exploited for the analysis of multitemporal optical (e.g., video surveillance), medical (disease-related changes detection, medical diagnosis and treatment) or acoustic images (under- water sensing) etc.

The most widely used types of unsupervised change detection techniques are based on the so called image difference [4]. These techniques generally require three steps [2].

First an essential image pre-processing of the input multitemporal images is necessary. In addition to the essential geometrical rectification and image co-registration step, and assuming that multitemporal images are from the same sensor, it includes handling the issues related to radiometric, atmospheric, noise and distortion corrections. Radiometric corrections are applied to the raw input images to correct for brightness values, of the different objects lying on the ground, that have been distorted because of sensor calibration/malfunction problems, or to rectify errors caused by the variation in sensor characteristics, solar angle, sensor view angle (to maintain the radiometric consistency) and atmospheric condition and phonological difference associated with seasonal variations. Image noise corrections is also sometimes necessary, especially in SAR (Synthetic Aperture Radar) images which may suffer from speckle noise at different levels when they are taken at different times [1]. Finally, Image distortion corrections are required to prevent the scattering difference of reflected electromagnetic light energy due to a constantly changing atmosphere.
In the second step, the two corrected and coregistred temporal image at two different times (but originating from the same sensor) are compared pixel by pixel in order to generate the so-called difference image by differencing (subtraction operator) or (log-)rationing ((log-)ratio operator). This latter difference image is such that the values of the pixels associated with land-cover changes present gray-level values significantly different from those of pixels associated with unchanged areas.
Finally, in the third step, is the classification or segmentation step on the difference image to distinguish between the changed and no changed areas. To this end, automatic binary thresholding methods have been proposed in order to determine the optimal threshold, in the sense of a given criterion.

In such a context, assuming that the first image co-registration and correction preprocessing step is successfully achieved, it is generally well known that the overall performance related to the change detection methods, based on the difference image, is mainly relied on the quality of the difference image and the accuracy of the classification method [6].

In order to efficiently address these two issues, this work proposes to first estimate, a new and robust similarity feature map, more reliable than the simple difference image,

978-1-4673-8910-5/16/$31.00 ©2016 IEEE

by specifying a set of constraints expressed for each pair of pixels existing in the two multitemporal images. As a consequence, the proposed change detection method does not require any preprocessing step of the multitemporal images such as radiometric, atmospheric and distortion corrections. In addition, input data can be acquired from different sensors. Only a co-registration between the two multitemporal images nevertheless remains necessary. The quadratic complexity, in the number of pixels, of the estimation of this new similarity feature map, between the multitemporal images, is reduced, in our approach, to an almost linear complexity procedure thanks to the FastMap algorithm.
Second, in order to achieve more robustness, changes are then identified, from this similarity feature map, by combining (fusing) the results of different automatic thresholding algorithms. In this way, we are able to exploit the properties of the different thresholding algorithms and to take into account or to combine the different criteria, for which these binary segmentation algorithms have been designed to be optimal in order to further increase the robustness and reliability of our proposed scheme.

In summary, the first originality of the proposed approach lies in the use of a new and original modeling involving the set of pair of pixels existing in the before and after satellite image. This property allows the difference image of the proposed change detection method to be robust to any imaging, noise modalities and degree of noise and eventually different sensors. The second originality of the approach is to reduce the quadratic complexity of this approach based on pixel pairwise to a linear complexity procedure, thanks to a modification of the FastMap-based optimization algorithm. Finally, the third originality lies in the fusion (or combination) of the results of different automatic thresholding algorithms on this difference image in order to quickly estimate a reliable change detection map.

The remainder of this paper is organized as follows: Sections II and III describe respectively the proposed change detection model and the optimization procedure related to this model. Section IV presents the fusion segmentation step. Finally, section V presents a set of experimental results.

II. Proposed Change Detection Model

Let us consider the two multitemporal remote sensing images (namely before and after change), y^1 and y^2 (of size N pixels) and acquired in the same geographical area at two different times; t_1 and t_2, and the subscript s indicates the spatial location. Let us assume that these two images have been correctly co-registered. Nevertheless, they can be acquired from different sensors and are possibly not corrected, in terms of radiometric, atmospheric and distortion consistencies and characteristics. Let y^D be our similarity feature map, playing the same role as the difference image, but more reliable than the simple difference image since this map will be estimated, not by pixelwise difference between y^1 and y^2 but by specifying a set of constraints expressed for each pair of pixels or sites $< s, t >$ existing in each two multitemporal images. In this model, our similarity map y^D can be seen as a solution to the following cost function to be optimized:

$$\hat{y}^D = \arg\min_{y^D} \sum_{<s,t>_{s\neq t}} \left(\beta_{s,t} - \left\|y_s^D - y_t^D\right\|_2\right)^2 \qquad (1)$$

where the summation $\sum_{<s,t>_{s\neq t}}$ is done over all the pairs of sites existing in our similarity feature image y^D to be estimated. In Eq. (1), the set of $\beta_{s,t}$, represents the set of $N(N-1)/2$ constraints expressed for each pair of pixels $<s,t>$, in terms of grey level differences in order to obtain a reliable similarity feature image y^D in which unchanged pixels will be associated to small gray-level values whereas changed pixels will present rather large values.

Let us recall that y^1 and y^2 are the two multitemporal remote sensing images (namely before and after change). First, let us assume that two pixels at sites s and t ($s \neq t$) belong to the class "urban" at time t_1 and they both belong still in the same class "urban", at time t_2. In this case, these two pixels should both belong to the (same) class label "unchanged pixels" and should also present both, a zero difference value, in terms of grey-level in y^D. This is expressed as follows:

CONSTRAINT #1: Two pixels at sites s and t ($s \neq t$) should belong to the class label "unchanged pixels" if y_s^1 and y_t^1 have the same grey level, **and** if y_s^2 and y_t^2 have also the same grey level. This belonging to the class "unchanged pixels" is all the more true that the distance $\beta_{s,t} = ||y_s^1 - y_t^1| - |y_s^2 - y_t^2||$ is small and in this case: A.] the distance, in terms of grey level difference, between y_s^D and y_t^D should be small (because s and t belong to the same class) and B.] y_s^D and y_t^D should present both small grey level values (i.e., a high probability of belonging to the "unchanged pixels" class expressed in y^D).

CONSTRAINT #2: Conversely, if the two pixels at sites s and t belong to a same class at time t_1 (for example "urban" for sites s & t and in this case; $|y_s^1 - y_t^1|$ is low) **and** a different class at t_2 (for example "water" for site s and"urban" for site t and in this case $|y_s^1 - y_t^1|$ is high) or conversely[1]. In that case, these two pixels should belong to a different class label in y^D; i.e., "unchanged pixels" for one of the two pixels and "changed pixels" for the other. This belonging to different class labels in y^D, for pixels s and t, is expressed, once again, in terms of grey level difference, by the distance $\beta_{s,t} = ||y_s^1 - y_t^1| - |y_s^2 - y_t^2||$ which has now become high (because of one of the two terms). In summary, the CONSTRAINT #1 and CONSTRAINT #2 can be expressed by:

$$\beta_{s,t} = \left||y_s^1 - y_t^1| - |y_s^2 - y_t^2|\right| \qquad (2)$$

Eq. (1) is in fact a composite cost function encoding our $N(N-1)/2$ constraints given by the *observed variables* y^1

[1]For example "water" for site s and"urban" for site t at time t_1 (and if this case $|y_s^1 - y_t^1|$ is high) and, at time t_2 "urban" for sites s and t (and if this case $|y_s^2 - y_t^2|$ is low).

and y^2. Optimization of Eq. (1) will ensure a robust similarity feature map $\hat{y}^D$ with land cover changes presenting significantly different values from those associated to the pixels belonging to unchanged areas. Nevertheless, it is important to note that the estimation of $\hat{y}^D$ does not guarantee that the constraint $\#1.B$ is satisfied. It follows that unchanged pixels in $\hat{y}^D$ will present either small grey-values, whereas changed pixel will present rather large values or conversely. In our case, this ambiguity can be easily resolved with a correlation metric or more simply by assuming that the land cover change is much smaller than the unchanged area.

III. FastMap-Based Model Optimization

Let us note that the function to be minimized (Eq. (1)) is also the so-called *stress* function used as a criterion in the mapping based on multidimensional scaling (MDS) technique [19]. MDS has already been successfully used in a number of practical applications, such as color image segmentation [12], [14], hyperspectral compression [13], asymmetry detection [15], human action recognition [16]. In our case, MDS is able to estimate a mapping, in our case, a grey-level similarity image y^D, such that the distances between each pair of grey-level values associated to pixels s and t are close of $\beta_{s,t}$ as faithfully as possible (in the least square sense). Nevertheless, the originally proposed MDS algorithm (called *metric MDS* [19]) is not appropriate in our application (and more generally for all large scale applications) because it requires an entire $N \times N$ distance matrix to be stored in memory with a $O(N^3)$ complexity (N being the number of pixels). Instead, we have herein adopted a fast alternative, called FastMap [20] whose main advantage is its linear complexity compared to the other metric MDS procedures.

However, the price paid for its low linear complexity is its sensitivity to outliers and non-linearities. In our case, this characteristic may give a poor or noisy estimation of our similarity image y^D. In order to get a more reliable estimation, an interesting solution is obtained by averaging the estimations from different pivot lines[2]. To this end the linear heuristic and deterministic procedure proposed by Falutsos and Lin can be easily modified in order to propose more than one pivot line.

IV. Fusion-based Segmentation Step

Finally, in order to achieve more robustness, changes are then identified, from the (previously estimated) similarity image y^D, by combining (fusing) the results of $T = 5$ different automatic thresholding algorithms[3] (namely [7], [8], [9], [10], [11]). In this way, this strategy (already been used in [5]) allows us to synergistically integrate multiple different criteria, for which these binary segmentation algorithms have been designed to be optimal in order to further increase the robustness and reliability of our proposed segmentation scheme. In our application, this binary fusion process is simply achieved by using a median filter using a three dimensional window $W \times W \times T$ whose the first two dimensions are spatial and the third dimension indexes the different binary thresholded maps to be fused.

V. Experimental Results

To validate our approach, we present in this section a set of experimental results obtained on different real, publicly available, optical, multi-temporal, multispectral, airborne SAR or radar data sets with available ground truth.

A. Dataset Description

The first dataset[1] is a pair of optical satellite images produced by the EROS data center in southwest U.S., corresponding to a part of Reno-Lake Tahoe area of Nevada (acquired on Aug. 5, 1986, and Aug. 5, 1992), with size 200×200 pixels, captured by the Landsat Multi-spectral Scanner. The Burn images show a change that results from forest fire phenomena. The Cuts images show a change described by a decrease in the surface area of the lake that results from drought effects. The Dray Lake images show a change that corresponds to the beginning and culmination of drought conditions in the western U.S. The Surface disturbance images show increased surface disturbance due to construction or excavations for construction including road resurfacing or paving.

The second dataset [22] [23] [24] [25] [27] is provided by the Defense Research and Development Canada (DRDC), Ottawa (Canada), and are two multi-temporal SAR images, with size 290×350 pixels, acquired by the Radar-Sat SAR sensor respectively, in July 1997 during the summer flooding, and Aug. 1997 after the summer flooding.

The third dataset [22] [23] [24] [25] [21] is a pair of two multi-temporal SAR images with a size 301×301 pixels, acquired by the European Remote Sensing 2 (ERS-2) satellite SAR sensor. It presents a natural phenomenon, generally occurring during the rainy season, in the Switzerland area, near the city of Bern, in April 1999 before the flooding and in May 1999 after the flooding.

The fourth dataset [21] shows a pair of X-band airborne SAR (intensity) images acquired over a field in Beijing, China, on

[2] In our case, the FastMap can be viewed as a procedure aiming to find y^D, such that the distances between each pair of grey-level values associated to pixels s and t are close of $\beta_{s,t}$ as much as possible. To this end, we recall that the first step, and an essential element of the FastMap algorithm, is to select two objects (pixels or sites in our case) to form the projection line. These two pixels, also called pair of anchor nodes or pivots (or pivot line) are selected such that the distance ($\beta_{s,t}$ in our application) is maximal. To accomplish such a task Falutsos and Lin [20] proposed a linear heuristic algorithm, based on a deterministic procedure called choose-distant-objects. The second step is to project any other object (pixels) onto this orthogonal axis (pivot line) by employing the cosine rule.

[3] Let us note that the concept of combining classifiers for the improvement of the performance of individual classifiers is known, in machine learning field, as a committee machine or mixture of experts [17], [18]. In this context, Dietterich [18] have provided an accessible and informal reasoning, from statistical, computational and representational viewpoints, of why ensembles can improve results.

[1] http://geochange.er.usgs.gov/sw/changes/natural/reno-tahoe/

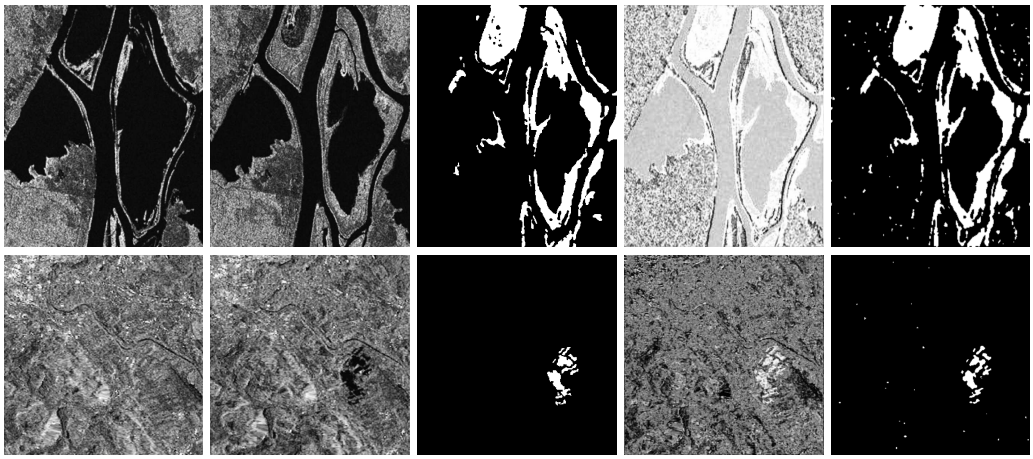

Fig. 1. Experimental results on SAR dataset: OTTAWA, BERN; From left to right; image acquired at time t_1 and t_2, ground truth, similarity feature map, final (changed/unchanged) binary segmentation result obtained by our approach.

Apr. 4 and 6, 2004.
The fifth dataset is a collection of images (with size 7660×7402 pixels), provided by the NASA/USGS Global Land Survey (GLS) [26], captured by the multispectral scanner Landsat-5 (Tm) and Landsat-t Enhanced Thematic Mapper Plus (ETM+) and showing various change phenomena in landscape, in different area, between 2000 and 2005. For each pair of image of the same area, this dataset proposes a ground truth image containing the different evolutions undergone by the area for five years (thrust drills, loss of trees, etc.).

B. Results & Evaluation

The quantitative analysis is done by the classification rate accuracy that calculate the percentage of the correct changed and unchanged pixels:

$$\text{PCC} = \frac{\text{TP+TN}}{\text{TP+TN+FN+FP}} \tag{3}$$

where TP, TN, FN, FP are respectively the number of pixels that are detected as the changed area in both the ground truth image and the machine result (True Positive), the unchanged area in both the reference image and the machine result (True negative), the changed pixels that are undetected (False negative) and finally the unchanged pixels wrongly classified as changed (False Positive).

Table 1 summarizes the different change detection accuracy rates obtained by our approach with a comparison with other state of the art approaches [22] [23] [24] [25] [21] [27] for different datasets with different imaging modalities (with the total number of images tested in each case). We can see that the different changed-unchanged detection binary map results match fairly the different regions present in the ground truth, and that the most changed regions for the different imagery modalities are well recognized by our strategy (see Fig. 1, 2, 3 and 4).

Method / Accuracy	Our	[22]	[23]	[24]	[25]	[21]	[27]
BERN dataset	.993	.997	.996	.996	.996	-	-
OTTAWA dataset	.943	.965	.974	.972	-	-	.988
SAR AIRBORNE dataset	.986	-	-	-	-	.997	-
Number of images tested	17	2	3	3	2	2	5

Table 1. Accuracy rate of change detection obtained by different state of the art methods, on BERN, OTTAWA, and SAR Airborne datasets.

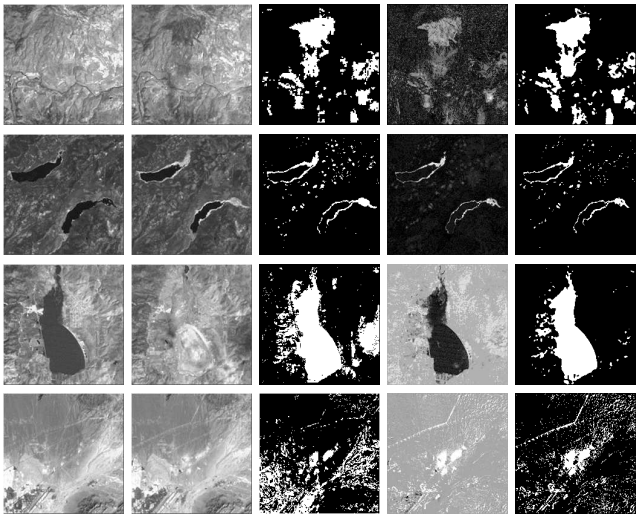

Fig. 2. Experimental results on optical Eros center dataset: BURN, CUTS, DRAY LAKE, SURFACE DISTURBANCE; From left to right; image acquired at time t_1 and t_2, ground truth, similarity feature map, final (changed/unchanged) segmentation result obtained by our approach.

We can also notice that the rate accuracy of our method remains comparable to the other "state of the art" approaches but above all that the strength of our model is its ability to process a wide variety of satellite imaging modalities (*i.e.*, multi-temporal, multispectral, airborne SAR or radar data) potentially degraded by different noise types and different noise levels (see, for example, the Fig. 1 where the SAR images are corrupted by different speckle noise levels). The

Fig. 3. Experimental results on SAR airborne dataset; From left to right; image acquired at time t_1 and t_2, ground truth; Second row: similarity feature map, final (changed/unchanged) binary segmentation result obtained by our approach.

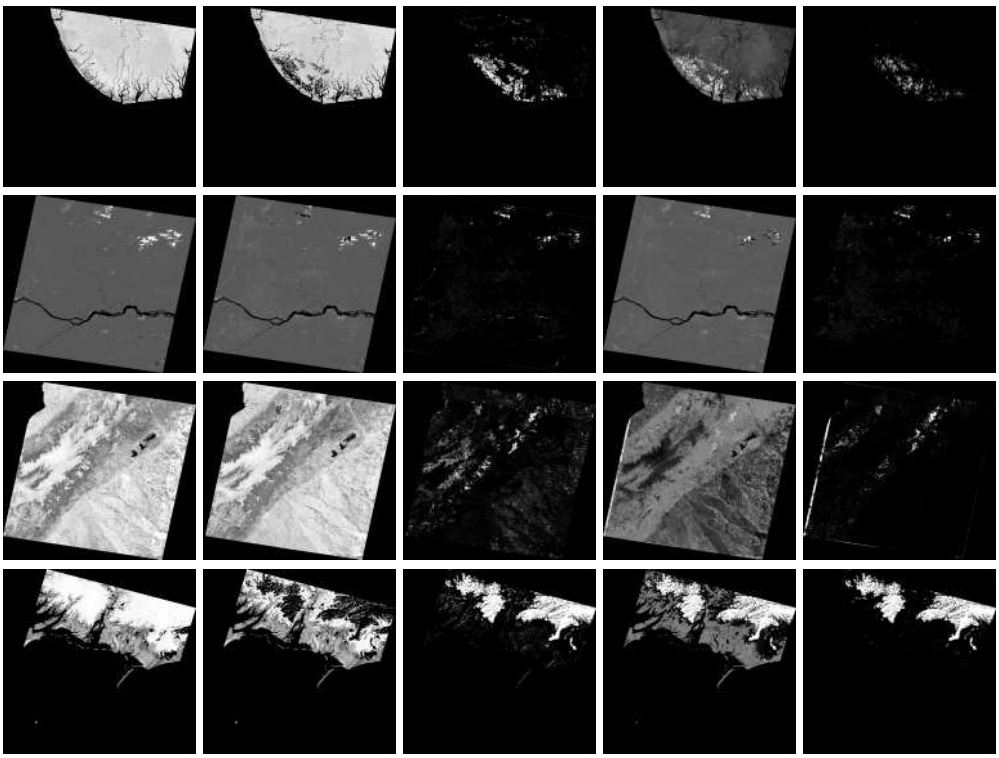

Fig. 4. Experimental results on Global land cover UMD-NASA dataset; From left to right; image acquired at time t_1 and t_2, ground truth, similarity feature map, final (changed/unchanged) binary segmentation result obtained by our approach.

accuracy rate obtained by our change detection approach over 17 image pairs stemming from the five different datasets described in Section V-A is $\rho = 0.94$.

VI. Conclusion

In this paper, we have proposed a novel change detection approach based on a new and robust similarity feature map which is defined by a set of constraints expressed for each pair of pixels existing in the multitemporal image pair. This estimation, based on a set of constraints between two pixels, allows us to define a new change detection method which does not require any preprocessing step of the multitemporal images such as radiometric, noise or distortion corrections/normalization. Besides, this estimation remains of linear complexity, in the number of pixels, thanks to the FastMap-based optimization algorithm and is made really accurate by fusing (averaging) the estimations obtained from different initializations (pivot lines). In order to achieve more robustness, changes are then identified, from this similarity feature map, by combining (fusing) the results of different automatic thresholding algorithms. Qualitative and quantitative results show that the proposed method consistently performs well, without preprocessing, on different types of input satellite images, degraded with possibly different types of noise or different level of noise, and showing different kind of changes due to different types of natural phenomena.

Acknowledgment

We would like to acknowledge the UMD and NASA to have prepared and made at our disposal the change detection dataset which allowed us to validate our algorithm. We would like also to acknowledge the Dr. Boli Xiong for sharing the SAR and SAR-airborne dataset used in this paper.

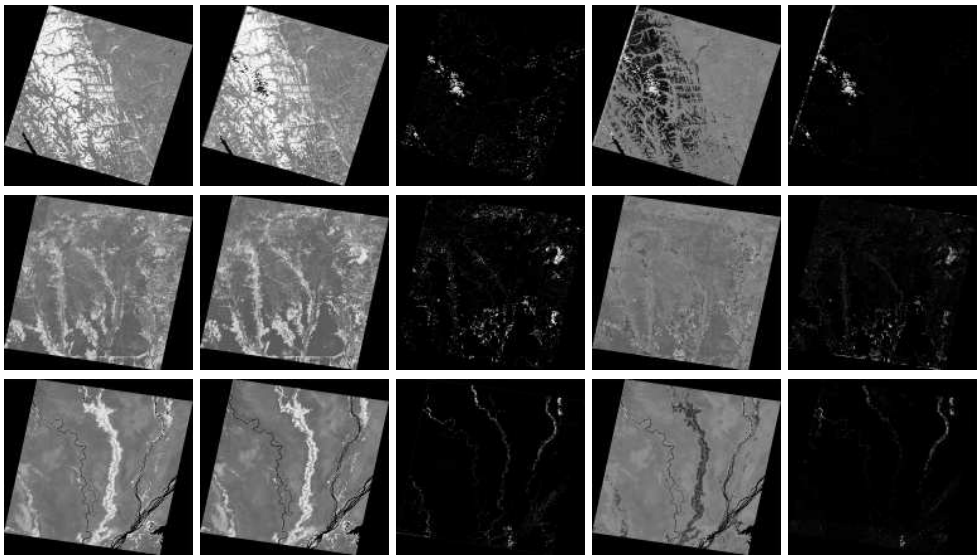

Fig. 5. Experimental results on Global land cover NASA dataset; From left to right; image acquired at time t_1 and t_2, ground truth, similarity feature map, final (changed/unchanged) binary segmentation result obtained by our approach.

REFERENCES

[1] J. Liu, M. Gong, Q. Miao, L. Su and H. Li. Change detection in synthetic aperture radar images based on unsupervised artificial immune systems. *Appl. Soft Comput.*, 34: 151–163, 2015.

[2] L. Bruzzone and D.F. Prieto. *An Adaptive Semiparametric and Context-based Approach to Unsupervised Change Detection in Multitemporal Remote-sensing Images*. *IEEE Transactions on Image Processing*, 11: 452-466, 2002.

[3] J.Shi, J.Wu, A.Paul, L.Jiao and M.Gong. Change Detection in Synthetic Aperture Radar Images Based on Fuzzy Active Contour Models and Genetic Algorithms. *Mathematical Problems in Engineering*, 2141–2151, 2014.

[4] L. Bruzzone and D. Fernndez-Prieto. Automatic analysis of the difference image for unsupervised change detection. *IEEE Transactions on Image Processing*,38: 1171–1182, 2000.

[5] F. Melgani and Y. Bazi. Robust Unsupervised Change Detection with Markov Random Fields. *IEEE International Geoscience & Remote Sensing Symposium, IGARSS 2006, July 31 - August 4, 2006, Denver, Colorado, USA, Proceedings*, 208–211, 2006.

[6] M. Gong, Z. Zhou and J. Ma. Change Detection in Synthetic Aperture Radar Images based on Image Fusion and Fuzzy Clustering. *IEEE Transactions on Image Processing*, 21: 2141–2151, 2012.

[7] J. Prewitt and M.L. Mendelsohn. The analysis of cell images. *Annals of the New York Academy of Sciences*, 128: 1035-1053, 1996.

[8] J.N. Kapur, P.K. Sahoo and A.K.C. Wong. A new method for gray-level picture thresholding using the entropy of the histogram. *Computer Vision, Graphics, and Image Processing*, 29: 273 - 285, 1985.

[9] G.W. Zack, W.E.Rogers and S.A. Latt. Automatic Measurement of Sister Chromatid Exchange Frequency. *Journal of Histochemistry and Cytochemistry*, 25: 741–753, 1977.

[10] J.C. Yen, F.J. Chang and S. Chang. Automatic Measurement of Sister Chromatid Exchange Frequency. *IEEE Transactions on Image Processing*, 4: 370-378, 1995.

[11] A.G. Shanbhag. Utilization of Information Measure as a Means of Image Thresholding. *CVGIP: Graphical Models and Image Processing*, 56: 414 - 419, 1994.

[12] M. Mignotte. MDS-based multiresolution nonlinear dimensionality reduction model for color image segmentation. *IEEE Trans. on on Neural Networks*, 22: 447-460, 2011.

[13] M. Mignotte. A bi-criteria optimization approach based dimensionality reduction model for the color display of hyperspectral images. *IEEE Trans. on Geoscience and Remote Sensing*, 50: 501-513, 2012.

[14] M. Mignotte. MDS-based segmentation model for the fusion of contour and texture cues in natural images. *Computer Vision and Image Understanding*, 116: 981-990, 2012.

[15] A. Moevus, M. Mignotte, J.A. de Guise and J. Meunier. A perceptual map for gait symmetry quantification and pathology detection. *BioMedical Engineering OnLine (BMEO)*, 14, 2015.

[16] R. Touati and M. Mignotte. MDS-based multi-axial dimensionality reduction model for human action recognition. *Eleventh conference on Computer and Robot Vision, CRV'2014*, 2014.

[17] A.J.C. Sharkey. Combining artificial neural nets ensemble and modular multi-net systems. *Springer-Verlag, New York, Inc., ISBN:185233004X*, 1999.

[18] T.G. Dietterich. Ensemble methods in machine learning. *Proceedings of the First International Workshop on Multiple Classifier Systems, LNCS, Multiple Classifier Systems*,1-15, 2000.

[19] T.F. Cox and M.A.A. Cox. Multidimensional Scaling. *Chapman & Hall, London*, 1994.

[20] C. Faloutsos and K.-I. Lin. FastMap: A Fast Algorithm for Indexing, Data-Mining and Visualization of Traditional and Multimedia Datasets. *Proceedings of the ACM SIGMOD International Conference on Management of Data*,163–174, 1995.

[21] B. Xiong, Q. Chen, Y. Jiang and G. Kuang. A Threshold Selection Method Using Two SAR Change Detection Measures Based on the Markov Random Field Model. *IEEE Geosci. Remote Sensing Lett*,9: 287–291, 2012.

[22] J. Lu, J. Li, G.Chen, L. Zhao, B. Xiong and G. Kuang. Improving Pixel-Based Change Detection Accuracy Using an Object-Based Approach in Multitemporal SAR Flood Images. *IEEE Journal of Selected Topics in Applied Earth Observations and Remote Sensing* ,8: 3486-3496, July, 2015.

[23] H. Li, M. Gong and J. Liu. A Local Statistical Fuzzy Active Contour Model for Change Detection. *IEEE Geoscience and Remote Sensing Letters* ,12: 582–586, March, 2015.

[24] M. Gong, Z. Zhou and J. Ma. Change Detection in Synthetic Aperture Radar Images based on Image Fusion and Fuzzy Clustering *IEEE Transactions on Image Processing* , 21: 2141 – 2151, 2012.

[25] J. Ma, M. Gong and Z. Zhou Wavelet Fusion on Ratio Images for Change Detection in SAR Images. *IEEE Geosci. Remote Sensing Lett.*, 9: 1122–1126, 2012.

[26] J.O Sexton, X.P. Song, M. Feng, P. Noojipady, A. Anand, C.Q. Huang, D.H. Kim, K.M. Collins, S. Channan, C. DiMiceli and J.R. Townshend. Global 30-m resolution continuous fields of tree cover: Landsat-based rescaling of MODIS vegetation continuous fields with lidar-based estimates of error. *Int. Journal of Digital Earth,*, 6(5), 427-448, 2013.

[27] M. Gong, J. Zhao, J. Liu, Q. Miao and L. Jiao. Change Detection in Synthetic Aperture Radar Images Based on Deep Neural Networks. *IEEE Transactions on Neural Networks and Learning Systems*, 27: 125–138, 2016.